Pfeiffer, D. R., & Deber, C. M. (1979) *FEBS Lett. 105*, 360–364.
Pfeiffer, D. R., & Chapman, C. L. (1984) *Biophys. J. 45*, 167a (Abstr. T-PM-D1).
Pfeiffer, D. R., Taylor, R. W., & Lardy, H. A. (1978) *Ann. N.Y. Acad. Sci. 307*, 402–423.
Pfeiffer, D. R., Chapman, C. L., Taylor, R. W., & Laing, J. L. (1983) *Inorg. Chim. Acta 79*, 214–215.
Rorabacher, D. B., Mackellar, W. J., Shu, F. R., & Bonavita, S. M. (1971) *Anal. Chem. 43*, 561–573.
Smith, G. D., & Kuax, W. L. (1976) *J. Am. Chem. Soc. 98*, 1578–1580.
Taylor, R. W., Kauffman, R. F., & Pfeiffer, D. R. (1982) in *The Polyether Antibiotics: Carboxylic Ionophores* (Westley, J. W., Ed.) pp 103–184, Marcel Dekker, New York.
Tissier, C., Julliard, J., Dupin, M., & Jeminet, G. (1979) *J. Chim. Phys. Phys.-Chim. Biol. 76*, 611–617.
Watts, A., Marsh, D., & Knowles, P. F. (1978) *Biochemistry 17*, 1792–1801.

n-Alkanols and Halothane Inhibit Red Cell Anion Transport and Increase Band 3 Conformational Change Rate†

Stuart A. Forman,* A. S. Verkman,‡ James A. Dix, and A. K. Solomon

Biophysical Laboratory, Department of Physiology and Biophysics, Harvard Medical School, Boston, Massachusetts 02115, and Department of Chemistry, State University of New York, Binghamton, New York 13901

Received January 23, 1985

ABSTRACT: The effects of halothane and *n*-alkanols on band 3, the anion-exchange protein of the red cell membrane, have been characterized by (1) radioactive sulfate exchange and (2) equilibrium and kinetic binding of a fluorescent anion transport inhibitor, 4,4′-dibenzamido-2,2′-stilbenedisulfonic acid (DBDS), with fluorescence and stopped-flow techniques. Ethanol, butanol, hexanol, heptanol, octanol, and decanol inhibit radioactive sulfate efflux from red blood cells in a dose-dependent manner with an average Hill coefficient of 1.3 ± 0.1. Over a 10^4-fold range of buffer concentrations, the calculated membrane alkanol concentrations at which anion transport rates are reduced by 50% are 100–200 mM. At 100–300 mM membrane concentrations, halothane and the *n*-alkanols increase the apparent rate of DBDS binding to band 3 2–3-fold. Analysis of kinetic and equilibrium DBDS binding data shows that these drugs increase the rate of the DBDS-induced conformational change in the DBDS–band 3 complex. Equilibrium DBDS binding studies reveal differences between the actions of short-chain alkanols (ethanol and butanol) and those of long-chain alkanols (hexanol and longer). Short-chain alkanols reduce the equilibrium affinity of DBDS for band 3, while long-chain alkanols have no effect on equilibrium DBDS binding. The results for halothane and long-chain alkanols suggest a nonspecific, lipid-mediated mechanism of anesthetic action, which may be coupled to protein inactivation by an increase in the rate of protein conformational changes resulting in nonfunctional states. The results for short-chain alkanols indicate that they have the same nonspecific actions as the long-chain alkanols but also have specific effects on the stilbene binding site of band 3.

General anesthetics are a structurally heterogeneous group of compounds, whose potencies correlate with oil/water (or membrane/buffer) partition coefficients (λ; Janoff & Miller, 1982; Meyer, 1937). Proposed mechanisms of action of anesthetics include changes in membrane fluidity (Metcalfe et al., 1968; Hubbell et al., 1970), membrane volume (Miller et al., 1973; Seeman & Roth, 1972), and lipid phase transitions (Hill, 1974; Trudell, 1977). Membrane proteins are assumed to mediate anesthetic-induced changes in functional properties such as transmembrane transport (Makriyannis & Fesik, 1980), receptor–ligand binding (Young & Sigman, 1981; Boyd & Cohen, 1984), and electrophysiologically observable channel dynamics (Gage et al., 1975). At present, the bulk lipid hypotheses of anesthetic action (fluidity, volume, and phase transitions) remain unproven, and in some experimental systems, a number of general anesthetic agents produce unexpected, drug-specific effects (e.g., short-chain alcohols enhance activation of postsynaptic cholinergic receptors at the neuromuscular junction; Gage et al., 1975). Recently, Franks & Lieb (1984) showed that anesthetics competitively inhibit ligand binding to a water-soluble protein. Other proposed sites of anesthetic action include hydrophobic sites within membrane proteins (Richards et al., 1978) and the boundary lipids adjacent to protein (Richards, 1976).

We have examined the interaction of halothane and the *n*-alkanols[1] with the red cell membrane protein band 3. We

† This investigation was supported by Office of Naval Research Contract N00014-83-K-0015. S.A.F. was supported by U.S. Public Health Service Award 2T32GM07753-06 from the National Institute of General Medical Sciences, J.A.D. by NIH HL29488, and A.K.S. by NIH HL14820.

‡ Present address: Division of Nephrology, Cardiovascular Research Institute, University of California, San Francisco, CA 94143.

[1] Abbreviations: DBDS, 4,4′-dibenzamido-2,2′-stilbenedisulfonic acid; DNDS, 4,4′-dinitro-2,2′-stilbenedisulfonic acid; pCMBS, *p*-(chloromercuri)benzenesulfonate; RBC, red blood cell; SITS, 4-acetamido-4′-isothiocyano-2,2′-stilbenedisulfonic acid; TCA, trichloroacetic acid. The term *n*-alkanol is used to represent a straight-chain alkane with a primary hydroxy group.

0006-2960/85/0424-4859$01.50/0

selected this model system because of availability and homogeneity of blood cells, the ease of preparation of membrane ghosts, and the existence of established assays for anion transport and inhibitor binding. Red cell membrane/buffer partition coefficients (λ^{RBC}) for alkanols (Seeman, 1972) and halothane (Smith et al., 1981) have been determined. Furthermore, the effects of alcohol and volatile anesthetics on red cell membrane fluidity, phase behavior, and volume have been characterized (Goldstein, 1984). Band 3 has been shown to function as a transmembrane anion exchanger. It is present in the red cell membrane as approximately 6×10^5 noncovalent dimers (monomer M_r 95K), comprising 25% of the membrane protein [for review, see Knauf (1979)].

Red cell anion exchange is blocked by stilbenedisulfonic acids (Cabantchik & Rothstein, 1972), phloretin (Forman et al., 1982), local anesthetics (Gunn & Cooper, 1975; Feinstein et al., 1977), and general anesthetics (Schnell, 1972; Makriyannis & Fesik, 1980; Motais et al., 1980; Abu Salah et al., 1982). Studies have shown that general anesthetic inhibition of sulfate (SO_4^{2-}) exchange is noncompetitive both with anion substrate binding (Schnell, 1972; Motais et al., 1980) and with inhibition by a stilbene inhibitor, 4-acetamido-4′-isothiocyano-2,2′-stilbenedisulfonic acid (SITS) (Abu Salah et al., 1982). While many general anesthetics are known to block red cell anion transport, previous studies have tested few drugs with known λ^{RBC}'s, precluding any critical evaluation of lipid-based mechanisms.

This paper reports studies on the mechanism of general anesthetic action on band 3 mediated anion transport. To test the membrane lipid hypotheses, the inhibition of anion transport ([^{35}S]sulfate exchange at equilibrium) by the family of *n*-aliphatic alcohols (*n*-alkanols), encompassing a 10^4-fold range of solution concentrations, was analyzed. In addition, the effects of the *n*-alkanols and the inhalation anesthetic halothane on the binding of the reversible anion transport inhibitor 4,4′-dibenzamido-2,2′-stilbenedisulfonic acid (DBDS) to band 3 were characterized. Stilbenedisulfonic acids have been used extensively to study the mechanism of RBC anion exchange. These membrane-impermeable agents competitively inhibit anion exchange only from the extracellular side of the membrane (Cabantchik & Rothstein, 1974) by binding at one site per band 3 monomer (Lepke et al., 1976; Ship et al., 1977), which is thought to be near the anion transport site (Macara & Cantley, 1981). Equilibrium DBDS binding to red cell membrane ghosts was measured by a fluorescence-enhancement titration. The rate of fluorescence enhancement caused by DBDS binding to band 3 in red cell membrane ghosts was measured by the stopped-flow rapid-mixing technique. Results of DBDS binding studies were analyzed according to the mechanism given by Verkman et al. (1983).

Materials and Methods

Chemicals. DBDS was synthesized by the method of Kotaki et al. (1971), and its purity was checked by thin-layer chromatography on silica gel G (Whatman, Inc., Clifton, NJ) in pyridine/acetic acid/water (10:1:40). 4,4′-Dinitro-2,2′-stilbenedisulfonic acid (DNDS) was purchased from K and K Laboratories or ICN Pharmaceuticals (Plainview, NY). Halothane (2-bromo-2-chloro-1,1,1-trifluoroethane) was a gift from Dr. E. Fossel. ^{35}S-Labeled H_2SO_4 was purchased from New England Nuclear (Boston, MA). The *n*-alkanols (ethanol, butanol, hexanol, heptanol, octanol, and decanol) and other reagents were purchased from Sigma Chemical Co. (St. Louis, MO). All *n*-alkanols were >99% pure.

Ghost Preparation. Hemoglobin-free, unsealed red cell ghost membranes were prepared from recently outdated blood by a modification of the method of Dodge et al. (1963). Blood was washed 3 times in 155 mM NaCl, hemolyzed in 5 mM sodium phosphate at pH 8.0, washed 4 times in phosphate buffer, and then washed twice in citrate buffer (28.5 mM sodium citrate, pH 7.4). Ghosts were stored at 4 °C and used within 72 h of preparation.

Preparation of Anesthetic Solutions. Saturated stock halothane solution was prepared by stirring citrate buffer with an excess of halothane in a closed flask overnight at 25 °C. For stopped-flow kinetic experiments, solutions containing lower halothane concentrations were prepared just before use by mixing the stock halothane solution with citrate buffer. Halothane concentrations were determined to ±2% by gas chromatography (Beckman Model 72, Palo Alto, CA). Less than 5% evaporation of halothane occurred between solution preparation and the end of stopped-flow data collection. Equilibrium binding and anion transport inhibition studies were not performed with halothane, because greater than 50% evaporated during the experiments.

Solutions of ethanol, butanol, hexanol, and heptanol were prepared by weighing *n*-alkanols into sealed volumetric flasks and stirring overnight in citrate buffer or sulfate flux buffer at 25 °C. *n*-Alkanol concentrations down to 2 mM were assayed by a microdiffusion technique in a Conway diffusion cell (Barnard & Chaysen, 1965). Solutions of octanol and decanol were prepared with known weights of *n*-alkanol first dissolved in ethanol; the ethanol solution was then diluted in buffer. The maximum final ethanol concentration was less than 1% v/v (170 mM), which was shown to have no effect on DBDS binding or sulfate efflux in control experiments.

Sulfate Efflux Experiments. Fresh human red cells were washed 3 times with sulfate flux buffer (150 mM NaCl, 5 mM KCl, 1 mM $MgCl_2$, 0.25 mM $CaCl_2$, 5 mM Na_2HPO_4, 1 mM NaH_2PO_4, 10 mM Na_2SO_4, and 10 mM glucose, pH 7.4). Cells were incubated with 0.5–1 μCi/mL $^{35}SO_4^{2-}$ for 3 h and then cooled on ice. The $^{35}SO_4^{2-}$-containing cells were washed 3 times with sulfate flux buffer at 4 °C, pelleted in a microcentrifuge (Brinkman Model 3200, Westbury, NY), and then resuspended at 35% hematocrit in sulfate flux buffer on ice. Sulfate efflux was initiated by diluting 1 mL of the 35% hematocrit suspension in 15 mL of sulfate flux buffer containing *n*-alkanols at 37 °C. Reaction vessels were sealed, except while solution was being withdrawn. Aliquots of 1 mL of the cell suspension were withdrawn at set times and centrifuged for 15 s (Brinkman Model 3200), and 0.3 mL of supernatant was counted (Tracor Analytic Model 6890, Elk Grove Village, IL) in 5 mL of Aquasol scintillation fluid (New England Nuclear, Boston, MA). An infinite time point was determined by trichloroacetic acid (TCA) hemolysis and precipitation of 1 mL of the cell suspension. Counts from the TCA experiments were corrected for dilution and quenching. Control experiments showed that TCA did not alter SO_4^{2-} binding to precipitated RBC's.

Equilibrium DBDS Binding. Equilibrium binding of DBDS to ghosts in the presence of *n*-alkanols was measured by the method of Verkman et al. (1983). Aliquots (5–10 μL) of DBDS solutions were sequentially added to a cuvette containing 3 mL of continuously stirred 0.03 mg/mL membrane protein ghost solution (40 nM band 3) at 25 °C. The 90° fluorescence of DBDS (excitation 360 nm, emission 414 nm) was monitored in a perkin-Elmer MFP-2A spectrofluorometer (Norwalk, CT) interfaced to a PDP 11/34 computer (Digital Equipment Corp., Maynard, MA). Raw fluorescence data were corrected for ghost scattering, fluorescence of unbound DBDS, inner filter effects, and dilution.

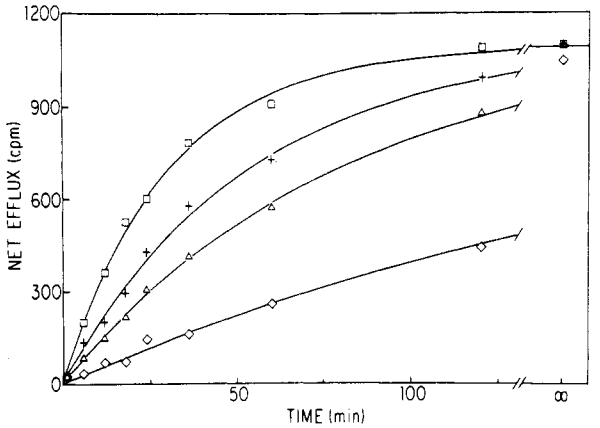

FIGURE 1: Effect of hexanol on sulfate efflux from red cells. The time course of appearance of radioactivity in the supernatant, determined as described under Materials and Methods, is shown for [hexanol] = 0 (□), 5.2 (+), 10.4 (△), and 19.5 mM (◇). Plotted curves are nonlinear least-squares fits to single exponentials, with infinite time points constrained to the radioactivity determined by TCA precipitation of cells. The exponential time constants are 29.7 ± 0.1, 52.7 ± 0.1, 79.7 ± 0.2, and 201 ± 10 min for increasing hexanol concentrations.

Stopped-Flow Experiments. Stopped-flow experiments were performed as described in Verkman et al. (1983), either on a laboratory-built apparatus (Verkman et al., 1981) interfaced to the PDP 11/34 computer or on a Dionex D-130 stopped-flow photometer (Sunnyvale, CA), interfaced with a PDP 11/23 computer (Digital Equipment Corp., Maynard, MA). Equal volumes of solutions containing ghosts (0.03 mg/mL protein) and DBDS (0.1–20 μM) were mixed, and the time course of fluorescence enhancement (excitation 350 nm, emission ≥400 nm) was measured with a photomultiplier tube. Halothane and *n*-alkanols were added to both the ghost and DBDS solutions. Stopped-flow experiments were performed at 25–27 °C.

Results

Transport Inhibition Studies. Figure 1 shows one experiment, typical of four, for hexanol effects on sulfate efflux. The time course of sulfate efflux is slowed as [hexanol] increases. The data fit single exponentials (<1% standard deviation), as expected for a steady-state, two-compartment system. Two washings in 10 volumes of buffer, following preincubation with 19.4 mM hexanol, returned the efflux rate to within 2% of control (two experiments, not shown), showing the anesthetic effect on anion transport is fully reversible.

Similar efflux time course data were obtained for ethanol, butanol, heptanol, octanol, and decanol. The percentage inhibition (% *I*) of SO_4^{2-} efflux was derived from the ratio of the exponential time constant in the absence of alkanol to the time constants in the presence of alkanol. The data are shown in Figure 2 as a function of buffer [*n*-alkanol]. The data were fitted, by a nonlinear least-squares procedure (Bevington, 1969), to a modified Hill equation (Waud, 1976):

$$\%\, I = \frac{[n\text{-alkanol}]^{n_H}}{[n\text{-alkanol}]^{n_H} + IC_{50}{}^{n_H}} \times 100 \qquad (1)$$

where n_H is the Hill coefficient and IC_{50} is the buffer [*n*-alkanol] producing 50% inhibition of efflux. Results of the fits are summarized in Table I.

The potency with which *n*-alkanols block anion exchange increases with chain length. The insert to Figure 2 shows a linear relation between log λ^{RBC} [2] (Seeman, 1972) and log IC_{50}

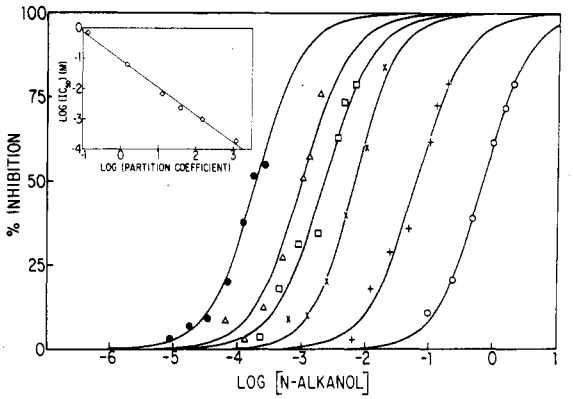

FIGURE 2: *n*-Alkanol dose dependence of sulfate flux inhibition. The percentage inhibition of sulfate efflux is plotted against log [*n*-alkanol] for ethanol (○), butanol (+), hexanol (×), heptanol (□), octanol (△), and decanol (●). Data were fitted to the Hill equation (eq 1), and fitted parameters are given in Table I. (Insert) A plot of log λ^{RBC} vs. log IC_{50} gives a line with slope −0.91 ± 0.05 (r = 0.996).

Table I: Effects of *n*-Alkanols on Sulfate Efflux

n-alkanol	λ^{RBC} (partition coeff)[a]	IC_{50} (M)[b]	n_H[b]	$\lambda^{RBC} \times IC_{50}$ (M)
ethanol	0.14[c]	0.70 ± 0.01	1.25 ± 0.04	0.098
butanol	1.5[c]	(6.4 ± 0.5) × 10^{-2}	1.17 ± 0.12	0.096
hexanol	13	(6.9 ± 0.4) × 10^{-3}	1.35 ± 0.10	0.090
heptanol	39.6	(2.3 ± 0.2) × 10^{-3}	1.16 ± 0.13	0.091
octanol	151.8	(1.0 ± 0.1) × 10^{-3}	1.50 ± 0.13	0.155
decanol	1222	(1.9 ± 0.1) × 10^{-4}	1.32 ± 0.08	0.232

[a] Partition coefficients are those reported by Seeman (1972). [b] IC_{50} and n_H are defined by eq 1. [c] Partition coefficient reported was calculated from the measured octanol/water partition coefficient as given by Seeman (1972).

with unity slope over 4 log units. This indicates a direct correlation between *n*-alkanol partitioning into red cell membranes and its ability to inhibit anion exchange. The membrane [*n*-alkanol] at 50% inhibition is calculated in Table I ($\lambda^{RBC} \times IC_{50}$).

The effect of hexanol on DBDS inhibition of sulfate efflux was examined. Dixon plots of SO_4^{2-} efflux time constant vs. [DBDS] (0–10 μM, data not shown) were analyzed by linear least squares. With no hexanol (r = 0.99), slope = 12.7 ± 0.2 μM^{-1} min, and y intercept = 28 ± 1 min; with 4 mM hexanol (r = 0.99), slope = 17.9 ± 0.9 μM^{-1} min, and y intercept = 41 ± 1 min. For a noncompetitive interaction between hexanol and DBDS, the fitted lines would intercept at a single point on the x axis, whereas a competitive interaction between *n*-alkanols and DBDS would give a single intercept on the y axis. The negative x intercepts of the weighted least-squares lines for 0 and 4 mM hexanol are 2.2 ± 0.1 μM and 2.3 ± 0.3 μM, respectively, consistent with a noncompetitive interaction between hexanol and DBDS.

Equilibrium DBDS Binding. DBDS is especially useful for examination of stilbene-bound band 3 states and conformation changes. DBDS binds reversibly and with high specificity to the stilbene inhibitor site, where it inhibits anion exchange (K_I

[2] Reports of partition coefficients (λ), especially those for short-chain alkanols, vary with the membrane used for the measurements (Miller, 1984). We have chosen to use those reported by Seeman (1972), because they are the only self-consistent set of measurements of alkanol partition coefficients in red cell membranes. Furthermore, they display chain-length dependence similar to measurements in other membranes. For example, a comparison of four alkanol λ's from Seeman (1972) with λ's measured in pure phospholipid membranes [from Pringle et al. (1981)] shows a relatively constant ratio: $\lambda^{PL}/\lambda^{RBC}$ = 2.5 ± 1.0.

= 1.3 ± 0.5 μM; Barzilay & Cabantchik, 1979) and undergoes a 100-fold increase in fluorescence quantum yield (Cabantchik & Rothstein, 1972; Rao et al., 1979). These features of the DBDS–band 3 interaction have enabled studies of equilibrium DBDS binding (Dix et al., 1979), the mechanism of DBDS binding (Verkman et al., 1983), and the effects of chloride (Verkman et al., 1982), phloretin (Forman et al., 1982), and pCMBS (Lukacovic et al., 1984) on DBDS-bound band 3 conformational states.

Verkman et al. (1983) proposed a mechanism of DBDS binding to band 3 dimers, summarized in eq 2. A fast [(1–5) $\times 10^{-6}$ M^{-1} s^{-1}] bimolecular association between DBDS and band 3 is followed by a slow (2 s^{-1}) band 3 conformational change. In the absence of transportable anions, a second DBDS binding step can also be seen. (Band 3)$_2$ represents a band 3 dimer. K_1 and K_3 are bimolecular dissociation constants, which characterize the two DBDS binding steps. k_2 and k_{-2} are forward and reverse rate constants for the DBDS–band 3 conformational change. Since the mechanism of DBDS binding involves two additions of DBDS to (band 3)$_2$, equilibrium binding is characterized by two equilibrium binding constants, K_1^{eq} and K_2^{eq}, defined as

$$\text{(band 3)}_2 \xrightarrow{K_1} \text{(band 3)}_2\text{DBDS} \underset{k_{-2}}{\overset{k_2}{\rightleftharpoons}} \text{(band 3)}_2\text{*DBDS} \xrightarrow{K_3} \text{(band 3)}_2\text{(DBDS)}_2 \quad (2)$$

(DBDS above K_1 and DBDS above K_3)

$$K_1^{eq} = \frac{[(\text{band 3})_2][\text{DBDS}]}{[(\text{band 3})_2\text{DBDS}] + [(\text{band 3})_2\text{*DBDS}]} = \frac{K_1}{1 + k_2/k_{-2}} \quad (3)$$

$$K_2^{eq} = \frac{[(\text{band 3})_2\text{DBDS}] + [(\text{band 3})_2\text{*DBDS}]}{[(\text{band 3})_2(\text{DBDS})_2]} = K_3(1 + k_{-2}/k_2) \quad (4)$$

With the assumption that all DBDS molecules bound to band 3 fluoresce with equal quantum yield, the sequential binding reaction scheme in eq 2 leads to the following dependence of corrected fluorescence, I_f, to [DBDS], K_1^{eq}, and K_2^{eq}:

$$I_f = \alpha\frac{K_2^{eq}[\text{DBDS}] + 2[\text{DBDS}]^2}{K_1^{eq}K_2^{eq} + K_2^{eq}[\text{DBDS}] + [\text{DBDS}]^2} \quad (5)$$

α is the fluorescence intensity of bound DBDS when bound to half of the total DBDS binding sites present (i.e., one DBDS molecule per band 3 dimer).

I_f vs. [DBDS] curves were fitted to eq 5 by nonlinear least squares with α, K_1^{eq}, and K_2^{eq} as fitting parameters. Previous experiments (Verkman et al., 1983) have shown that K_1^{eq} and K_2^{eq} determined by the fluorescence assay agree with equilibrium binding constants determined by a centrifugation method in which *unbound* DBDS was quantified. To test the sensitivity of the method for detecting changes in high-affinity DBDS binding to ghosts, fluorescent titrations were performed in the presence of DNDS, a stilbene inhibitor that competitively blocks DBDS binding to band 3. At 0, 2.5, and 5.0 μM DNDS, fitted K_1^{eq} values were 58 ± 18 nM, 198 ± 35 nM, and 420 ± 120 nM, respectively. A fit of K_1^{eq} vs. [DNDS] to a line (r = 0.99) gave a negative x intercept of 0.8 ± 0.1 μM, consistent with previously determined DNDS dissociation constants of 0.59 μM (Fröhlich, 1982) and 0.87 μM (Barzilay & Cabantchik, 1979). K_2^{eq} is not well determined (±200% in some cases) by fluorescence methods because of large inner filter effects with DNDS and high [DBDS]. The large errors in K_1^{eq} (see also Table II) are in part the result of the poor fit for K_2^{eq}. To test the model dependence of our analysis, the corrected fluorescence results from the DNDS experiments were fitted to a single-site model (eq 5a).

$$I_f = 2\alpha\frac{[\text{DBDS}]^{n_H}}{[\text{DBDS}]^{n_H} + K_{50}^{eq\,n_H}} \quad (5a)$$

In this model, only a single DBDS dissociation constant, K_{50}^{eq}, is specified, as well as α and n_H. The nonlinear least squares fitted K_{50}^{eq} values were 155 ± 7 nM, 590 ± 20 nM, and 1200 ± 300 nM, for increasing [DNDS]. A linear least-squares fit of K_{50}^{eq} vs. [DNDS] gave a negative x intercept of 0.6 ± 0.1 μM, consistent with the results of the two-site model. Thus, the fluorescence titration method is sensitive to changes in high-affinity DBDS binding to band 3, regardless of whether the two-site model of Verkman et al. (1983) is used. However, with the single DBDS site model, the average Hill coefficient from the nonlinear least-squares fits was 0.8 ± 0.05, indicating the presence of low-affinity binding.

Figure 3 shows corrected fluorescence binding data for three ethanol concentrations with fitted curves obtained from eq 5. As ethanol concentration increases, K_1^{eq} increases, as shown by the higher [DBDS] required to reach half-maximal I_f. The limiting value of I_f at high DBDS is independent of ethanol concentration, suggesting that the quantum yield of bound DBDS is unaffected by the presence of ethanol in the mem-

Table II: Effects of *n*-Alkanols on DBDS Binding to Ghosts

n-alkanol	solution concn (mM)	membrane concn (mM)[a]	K_1^{eq} (nM)
control (no alcohol)	0	0	51 ± 5
ethanol	250	35	69 ± 20
	500	70	124 ± 36
	1500	210	400 ± 120
	2000	280	460 ± 130
butanol	110	165	158 ± 35
	220	330	813 ± 168
hexanol	9.3	120	44 ± 13
	14	180	46 ± 14
	18.7	240	87 ± 23
heptanol	6.9	270	71 ± 61
octanol	1.0	150	52 ± 15
	2.0	300	78 ± 24
decanol	0.26	320	63 ± 48

[a] Membrane concentrations were calculated with λ^{RBC}'s from Table I.

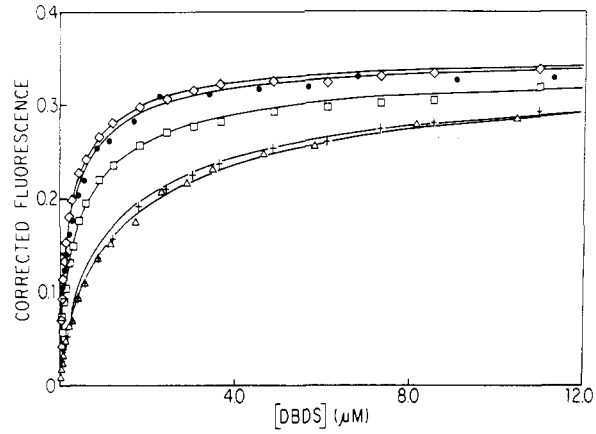

FIGURE 3: Effect of ethanol on DBDS binding to red cell ghosts. Corrected fluorescence, F, is plotted against [DBDS] for a control experiment (◇) and four ethanol concentrations: 0.25 (●), 0.5 (□), 1.5 (+), and 2.0 M (△). Fitted curves were obtained from eq 5 by nonlinear least squares. K_1^{eq}'s are given in Table II. For increasing ethanol concentrations, fitted α values are 0.176 ± 0.005, 0.175 ± 0.005, 0.168 ± 0.007, 0.164 ± 0.006, and 0.172 ± 0.006, respectively.

Table III: Effects of Halothane and Octanol on DBDS–Ghost Binding Kinetics

anesthetic	solution concn (mM)	k_1^{app} (μM)	k_2^{app} (s^{-1})	k_{-2}^{app} (s^{-1})
halothane[a]	0	1.3 ± 0.2	1.7 ± 0.2	
	1.8	1.2 ± 0.2	2.3 ± 0.2	
	5.1	1.4 ± 0.2	3.0 ± 0.3	
	9.5	1.3 ± 0.1	3.7 ± 0.2	
octanol[b]	0	2.2 ± 0.8	2.1 ± 0.5	0.07 ± 0.02
	0.7	2.3 ± 0.9	3.2 ± 0.9	0.10 ± 0.04
	1.5	2.0 ± 0.9	5.5 ± 1.9	0.20 ± 0.05
	2.2	1.4 ± 0.3	5.9 ± 0.9	0.31 ± 0.08
	2.9	1.2 ± 0.3	6.4 ± 0.6	0.41 ± 0.10

[a] Kinetic parameters were calculated from τ vs. [DBDS] data taken in the presence of halothane (DBDS range 1–10 μM, not shown) by nonlinear least-squares fit to eq 7. [b] Kinetic parameters were calculated from τ vs. [DBDS] data as described in legend to Figure 4, bottom.

brane and that the total number of DBDS binding sites on ghost membranes is not affected by ethanol.

Table II shows the values of K_1^{eq} for several *n*-alkanols. For ethanol and butanol, there is an increase in K_1^{eq} with increasing alcohol concentration. For the longer chain alcohols, there is little effect on equilibrium binding of DBDS to red cell ghosts at membrane concentrations that affect K_1^{eq} for ethanol and butanol. Reversibility was tested by preincubating ghosts with ethanol and octanol, followed by washing in citrate buffer. Fluorescence titrations (three experiments for each alcohol, data not shown here) gave fitted parameters within ±15% of control values. As with ethanol, the longer *n*-alkanols had no effect on the apparent quantum yield of DBDS bound to band 3.

Stopped-Flow Kinetics. The mechanism of eq 2 predicts that the dependence of the stopped-flow time constant, τ (from single-exponential fits), on [DBDS] is given by eq 6 (Verkman

$$\tau^{-1} = k_{-2} + \frac{k_2[\text{DBDS}]}{K_1 + [\text{DBDS}]} \quad (6)$$

et al., 1983) when [DBDS] ≫ [band 3]. In the limit of $k_2 \gg k_{-2}$ at high [DBDS], eq 6 simplifies to give a linear relation between τ and $[\text{DBDS}]^{-1}$:

$$\tau = \frac{K_1}{k_2[\text{DBDS}]} + \frac{1}{k_2} \quad (7)$$

For analysis of stopped-flow data taken in the presence of halothane and the *n*-alkanols, we define anesthetic-dependent parameters, K_1^{app}, k_2^{app}, and k_{-2}^{app}, and apply equations analogous to eq 6 and 7. Equation 7 was used for analysis of halothane or alkanol experiments. Equation 6 was used for alkanol experiments only, because K_1^{eq} values in the presence of alkanols were known (Table II), providing an additional constraint on the fit.

At a given DBDS concentration, halothane and the *n*-alkanols accelerate the time course of DBDS binding to ghost membranes. Figure 4, top, shows typical time courses in the absence and presence of octanol. There is a 4-fold increase of the DBDS binding rate constant, τ, in the presence of 2.0 mM octanol. Figure 4, bottom, shows the effect of octanol on DBDS–band 3 binding kinetics. It is apparent that τ decreases as [octanol] increases, especially at low [DBDS].

Table III summarizes the concentration-dependent effects of halothane and octanol on K_1^{app}, k_2^{app}, and k_{-2}^{app}. K_1^{app} does not significantly change with [halothane] or [octanol], while k_2^{app} increases from 2 to 4 s^{-1} in 10 mM halothane and to 6 s^{-1} in 3 mM octanol. With the data in Table III and λ^{RBC} = 36.5 for halothane [averaged from Smith et al. (1981) and Franks & Lieb (1981)], a linear least-squares fit of k_2^{app} vs.

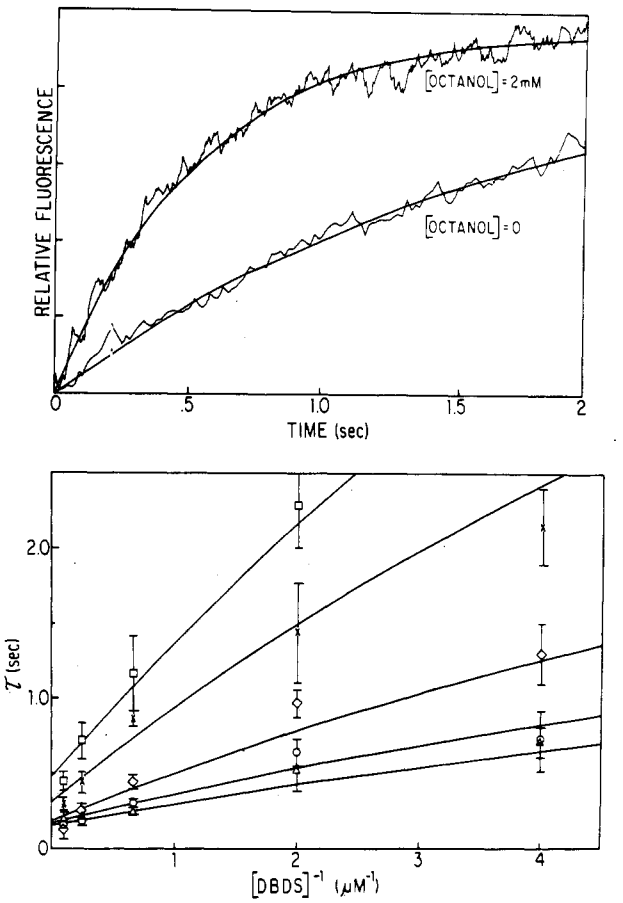

FIGURE 4: Effect of octanol on the time course of DBDS binding to red cell ghosts. (Top) In the experiment with octanol, 2.0 mM octanol was present in both ghost and 0.5 μM DBDS solutions prior to mixing. Digitized time courses (512 points) were fitted to single exponentials by nonlinear least squares. Fitted results: τ = 1.9 ± 0.5 s (0 mM octanol) and 0.5 ± 0.1 s (2 mM octanol). (Bottom) Stopped-flow time constant, τ, vs. $[\text{DBDS}]^{-1}$ is plotted, measured in the presence of octanol at 0 (□), 0.7 (×), 1.5 (◇), 2.2 (○), and 2.9 mM (△). The [DBDS] range was 0.1–10 μM, although 0.1 μM points are not shown. Error bars represent 1 SD for experiments performed at least in quadruplicate. Fitted lines were obtained by weighted least squares to eq 6, with the constraint that eq 3 was satisfied when K_1^{eq} = 60 nM. Fitted parameters are reported in Table III.

membrane [halothane] has a slope of 5.6 ± 0.7 M^{-1} s^{-1}. A similar calculation for k_2^{app} vs. membrane [octanol], with λ^{RBC} from Table I, gives a slope of 10.2 ± 1.6 M^{-1} s^{-1}.

In order to explore the effects of other *n*-alkanols on K_1^{app} and k_2^{app}, we measured τ values in quadruplicate at [DBDS] = 0.5 and 4 μM, as a function of *n*-alkanol concentrations. The results are shown in Figure 5, left. Values for K_1^{app} and k_2^{app} were calculated from $\tau_{c=4\mu M}$ and $\tau_{c=0.5\mu M}$ with eq 7. As shown in Figure 5, right, the *n*-alkanols have no significant concentration-dependent affect on K_1^{app}, whereas they increase k_2^{app}. The change in k_2^{app} depends upon the membrane [alkanol] as calculated from λ^{RBC}'s (Seeman, 1972), rather than upon solution [alkanol] or chain length. the slope of the least-squares line of k_2^{app} vs. membrane [alkanol] is 9.9 ± 2.0 M^{-1} s^{-1}, in agreement with the value derived from octanol alone.

Discussion

The red blood cell and the red cell membrane ghost preparation provide a model system in which anion transport function and stilbene inhibitor binding to band 3 can be studied. Drugs that affect band 3 function can be characterized by their effects on the equilibrium and kinetic binding of stilbene probes, providing information about effects on band

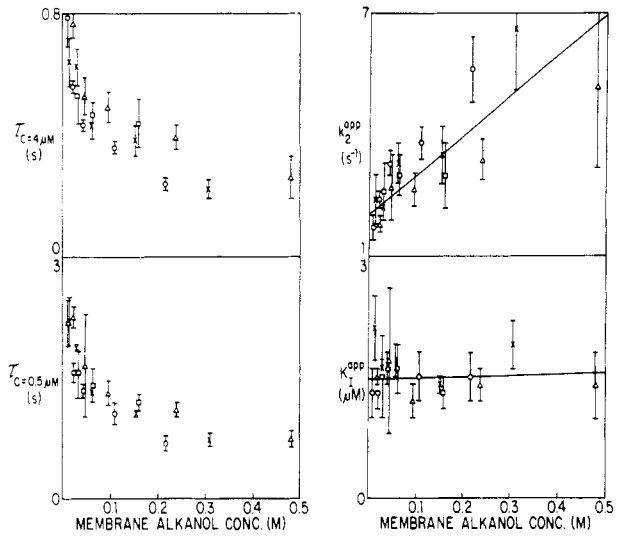

FIGURE 5: *n*-Alkanol effects on DBDS–band 3 kinetics. (Left) Effects of ethanol (○), butanol (□), hexanol (×), and octanol (△) on exponential time constants, $\tau_{c=4\mu M}$ and $\tau_{c=0.5\mu M}$ of DBDS binding to red cell ghosts. The abscissa is membrane [alkanol], calculated with λ^{RBC}'s from Seeman (1972). (Right) k_2^{app} and K_1^{app}, calculated from data in Figure 5, left, with eq 7, are plotted against membrane alkanol concentration. A weighted linear fit of k_2^{app} vs. membrane [alkanol] gives a slope of 9.9 ± 2.0 M^{-1} s^{-1} and an intercept of 2.0 ± 0.2 s^{-1}; K_1^{app} vs. membrane [alkanol] gives a slope of 0.2 ± 0.3 μM/M and an intercept of 1.5 ± 0.1 μM.

3 structural transitions. The work presented here is an analysis of the actions of the *n*-alkanols and halothane, which are known to alter red cell membrane structure, on band 3.

The *n*-alkanols reversibly inhibit anion transport by band 3, as measured by [^{35}S]sulfate efflux from red cells, in a manner consistent with a lipid-mediated mechanism. The dose–response curves exhibit Hill coefficients of 1.3 ± 0.1 (Figure 2). These Hill coefficients are higher than the value of 1.0 predicted by action at a single, saturable site. This may be due to a concentration-dependent increase in partitioning of alcohols into the red cell membrane (Colley et al., 1971) or to cooperativity in the mechanism that couples anesthetic binding to inhibition of anion exchange. However, there may be additional effects of alkanols on transmembrane sulfate flux in red cells. We observed 80–85% inhibition of sulfate flux by alkanols before some hemolysis of red cells was evident. Since leakiness to ions is known to occur at slightly lower, "prelytic" anesthetic concentrations (Seeman, 1972), the inhibition of sulfate efflux by alkanols is probably underestimated at our highest experimental concentrations. Correction for an anesthetic-dependent sulfate leak would, however, *increase* the apparent Hill coefficient.

The inhibitory potency of the *n*-alkanols correlates well with λ^{RBC}'s (Figure 2, inset) or with λ's measured in model membranes (see footnote 2). Multiplying the IC_{50}'s by λ^{RBC}'s (Table I, last column) shows that 50% inhibition of SO_4^{2-} efflux occurs at membrane [anesthetic] of 100–200 mM. This range is 1–5-fold higher than the membrane concentrations reported for 50% blockade of frog sciatic nerve action potentials (Seeman, 1972) and the EC_{50}'s (concentration at 50% effect) for general anesthesia in several animal models (Janoff & Miller, 1982). Although the Meyer–Overton rule is observed in our results, it does not constitute proof of a lipid-mediated anesthetic mechanism. For instance, there is direct evidence that benzyl alcohol binds to protein in red cell membranes (Colley et al.,, 1971) and its partition coefficient in red cell membranes is not fully accounted for by partitioning into purified membrane lipids.

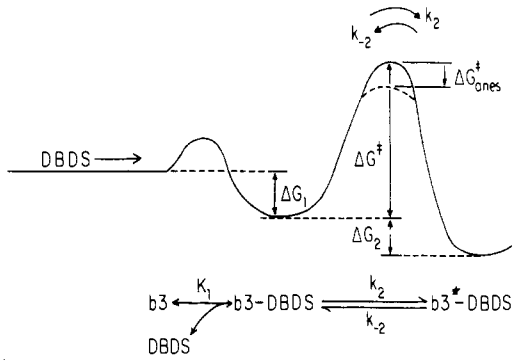

FIGURE 6: Schematic of thermodynamic potential for DBDS binding to band 3. Anesthetics accelerate the DBDS–band 3 conformational change, without altering equilibrium binding of DBDS by reducing $\Delta G^{\ddagger}$ by a concentration-dependent amount, $\Delta G^{\ddagger}_{anes}$, as shown.

Our studies on the combined effects of hexanol and DBDS on anion flux in red cells give results consistent with a noncompetitive interaction. Statistical evaluation of the negative *x* intercepts from Dixon plots for DBDS in the presence and absence of hexanol shows that these data may not represent a strictly noncompetitive interaction of the two inhibitors ($p < 0.4$). However, the data clearly show that the two agents are *not competitive*. This result is in agreement with that of Abu Salah et al. (1982), who found general anesthetics to be noncompetitive with another stilbene inhibitor, SITS.

Equilibrium binding of DBDS to band 3 is unaffected by long-chain ($n = 6$ and above) alkanols, as determined by fitted K_1^{eq} parameters from DBDS fluorescence enhancement titrations. Stopped-flow kinetic results indicate that both halothane and the *n*-alkanols (Table III and Figure 5) increase the apparent rate constant, k_2^{app}, for the band 3–DBDS conformational change. The change in k_2^{app} correlates with [alkanol] (Figure 5, right). Membrane concentrations of halothane producing a given change in k_2^{app} are comparable to those of the alcohols. Since we find that K_1^{eq} is unchanged by anesthetics, while k_2^{app} increases, we deduce that k_{-2}^{app} must also increase, maintaining a constant k_2^{app}/k_{-2}^{app} ratio (see eq 3). This result suggests that long-chain alkanols and halothane can lower activation barriers for protein conformational changes without altering relative stabilities of equilibrium conformational states.

A thermodynamic model, shown in Figure 6, illustrates how these effects of long-chain alkanols and halothane on DBDS binding may be produced. For simplicity, only the first DBDS binding step and the protein conformational change are contained in the reaction coordinate. The relative free energies of the states of the system and the activation energy for the conformational change are depicted by the various ΔG values. The value of K_1^{eq} depends only on ΔG_1 and ΔG_2, while k_2 and k_{-2} are determined by the rate-limiting transition-state free energy, $\Delta G^{\ddagger}$. Anesthetics reduce $\Delta G^{\ddagger}$ by a dose-dependent amount, $\Delta G^{\ddagger}_{anes}$, while ΔG_1 and ΔG_2 remain fixed. The result is faster forward and backward conformational change rates, k_2 and k_{-2}, while equilibrium binding is unchanged. The reversibility of anesthetic effecs shows that the induced changes in protein free energy are small relative to the total free energy stabilizing the native protein structure.

The actions of ethanol and butanol on DBDS binding to band 3 differ from those of long-chain alkanols, on the basis of fluorescence enhancement titrations. Like the longer alkanols and halothane, they increase the rate of DBDS binding to membrane ghosts, but ethanol and butanol cause a concentration-dependent reduction in equilibrium DBDS binding affinity to band 3 (Table II). When red cell membranes are

perturbed with short-chain alkanols, calorimetric scans of these membranes (Krishnan & Brandts, 1979) exhibit shifts in band 3 associated thermal transitions. This evidence supports the conclusion that short-chain alkanols perturb the band 3 equilibrium state. The small size of ethanol and butanol molecules may give them access to sites in proteins that the longer alkanols cannot enter. DBDS binding to band 3 has been shown to increase when buffer ionic strength is increased (Verkman et al., 1983), indicating an electrostatic component to binding. High concentrations of ethanol or butanol, by reducing the dielectric constant of buffer [about 2% decrease at 2 M ethanol, using the assumptions of Gage et al. (1975)], would decrease DBDS binding, although not to the extent observed. Alternatively, the actions of short-chain alkanols may differ from those of longer alcohols due to the tendency of shorter alcohols to concentrate near the membrane surface (Chin & Goldstein, 1981).

Differences between long- and short-chain alcohol effects have been observed in the neuromuscular junction and are attributed to changes in membrane dielectric constant (Gage et al., 1975) and specific binding of alcohols to protein (Bradley et al., 1984). In other model systems, such as the red cell glucose transport system (Lacko et al., 1973) and the *Torpedo* cholinergic receptor (Young & Sigman, 1981; Boyd & Cohen, 1984), many general anesthetics affect equilibrium binding of ligands to membrane protein. By use of the scheme in Figure 6, a simple model to explain the effects of short-chain alkanols on stilbene inhibitor binding to band 3 can be proposed. As with the longer alkanols, ΔG^* is reduced, but the short-chain alkanols may also reduce the size of ΔG_1, resulting in a lower equilibrium affinity of DBDS for band 3. Note that a decrease in ΔG_1 alone will also reduce the stability of the DBDS–band 3* state, which is determined by $\Delta G_1 + \Delta G_2$.

The acceleration of DBDS binding to band 3 is concentration dependent, with a 3-fold increase in k_2^{app} occurring in a narrow membrane [anesthetic] range (100–300 mM). In the same concentration range, anion transport by band 3 is reduced by 50–75%. Similar increases in the rates of membrane protein conformational changes by general anesthetics have been observed by others. Examples include channel closing in cholinergic receptors at the neuromuscular junction (Gage et al., 1975), desensitization of the *Torpedo* acetylcholine receptor (Young & Sigman, 1983), and both activation and inactivation of voltage-gated sodium channels (Haydon & Urban, 1983). The fact that acceleration of state transitions occurs in other model systems suggests that this may be an important effect of anesthetics on membrane proteins.

n-Alkanols and halothane decrease the lipid order parameter of model membranes with potencies proportional to their partition coefficients (Goldstein, 1984). There is abundant evidence that bulk protein movements, such as rotation and translation in the membrane bilayer, are accelerated by fluidization (decreasing order parameter) of membranes (Edidin, 1981). Thus, intraprotein motions, such as critical conformational changes, may also be accelerated by anesthetics through coupling of lipid and protein movements. However, the membrane order parameter does not generally correlate with the anion transport efficiency of red cells. Increased temperature, which also fluidizes membranes, increases the rate of anion exchange, while membrane fluidizing drugs inhibit anion transport.

Our results are consistent with a membrane fluidization model but do not rule out membrane expansion or phase-transition models of anesthetic action. However, models that couple membrane expansion or phase transitions with protein dynamics require a number of ad hoc assumptions. Models based on specific interactions of anesthetics with protein (and those invoking annular lipids) can account for exceptions to the rules defined by unitary lipid-based hypotheses. With additional assumptions, such models could also apply to our results, especially those for ethanol and butanol.

We put forward a new model of general anesthetic action, based on the acceleration of membrane protein dynamics. In our model, general anesthetics reduce membrane protein conformational transition energies, increasing conformational change rates that divert proteins into nonfunctional states. For example, when band 3 conformational changes are triggered by substrate binding in the presence of general anesthetics, the protein has a lower probability of following its normal reaction pathway, resulting in reduced transport efficiency. Small changes in transition-state stabilities and a large number of nonfunctional protein conformations could combine to reduce protein function without affecting equilibrium structure.

Increased temperature and anesthetics both accelerate protein dynamics but have opposite effects on function. In terms of our model, heat accelerates protein dynamics by increasing the available kinetic energy without necessarily changing the thermodynamic profile of protein structure. In contrast, anesthetics must act by altering the thermodynamic profile of protein structure in various ways. Our data suggest that one of these alterations is the reduction of certain transition-state free energies. This accelerated protein dynamic model is akin to the degenerate perturbation model of Richards et al. (1978) but adds to it an explicit mechanism for the reversible loss of protein function.

ACKNOWLEDGMENTS

We thank M. Toon for expertly preparing ghosts and performing protein concentration assays. We also thank Dr. Kieth Miller for helpful discussions on membrane/anesthetic interactions.

Registry No. Halothane, 151-67-7; ethanol, 64-17-5; butanol, 71-36-3; hexanol, 111-27-3; heptanol, 111-70-6; octanol, 111-87-5; decanol, 112-30-1.

REFERENCES

Abu Salah, K. M., Hampton, K. K., & Finday, J. B. C. (1982) *Biochim. Biophys. Acta 688*, 163.

Barnard, J. A., & Chaysen, R. (1965) *Modern Methods of Chemical Analysis*, pp 32–34, McGraw-Hill, London.

Barzilay, M., & Cabantchik, Z. I. (1979) *Membr. Biochem. 2*, 297–322.

Bevington, P. R. (1969) *Data Reduction and Error Analysis for the Physical Sciences*, McGraw-Hill, London.

Boyd, N. D., & Cohen, J. B. (1984) *Biochemistry 23*, 4023–4033.

Bradley, R. J., Sterz, R., & Peper, K. (1984) *Brain Res. 295*, 101–112.

Cabantchik, Z. I., & Rothstein, A. (1972) *J. Membr. Biol. 10*, 311–330.

Cabantchik, Z. I., & Rothstein, A. (1974) *J. Membr. Biol. 15*, 207–226.

Chin, J. H., & Goldstein, D. B. (1981) *Mol. Pharmacol. 19*, 425–431.

Colley, C. M., Metcalfe, S. M., Turner, B., Burgen, A. S. V., & Metcalfe, J. C. (1971) *Biochim. Biophys. Acta 233*, 720–729.

Dix, J. A., Verkman, A. S., Solomon, A. K., & Cantley, L. C. (1979) *Nature (London) 282*, 520–522.

Dodge, J. T. C., Mitchell, C., & Hanahan, D. J. (1963) *Arch. Biochem. Biophys. 100*, 119–130.

Edidin, M. (1981) in *Membrane Structure* (Finean, M., Ed.) pp 37–82, Elsevier/North-Holland Biomedical Press, New York.

Feinstein, M. B., Volpi, M., Perrie, S., Makriyannis, A., & Sha'afi, R. (1977) *Mol. Pharmacol. 13*, 840–851.

Forman, S. A., Verkman, A. S., Dix, J. A., & Solomon, A. K. (1982) *Biochim. Biophys. Acta 689*, 531–538.

Franks, N. P., & Lieb, W. R. (1981) *Nature (London) 292*, 248–251.

Franks, N. P., & Lieb, W. R. (1984) *Nature (London) 310*, 599–601.

Frölich, O. (1982) *J. Membr. Biol. 65*, 111–123.

Gage, P. W., McBurney, R. N., & Schneider, G. T. (1975) *J. Physiol. (London) 244*, 409–429.

Goldstein, D. B. (1984) *Annu. Rev. Pharmacol. Toxicol. 24*, 43–64.

Gunn, R. G., & Cooper, J. A. (1975) *J. Membr. Biol. 25*, 311–326.

Haydon, D. A., & Urban, B. (1983) *J. Physiol. (London) 341*, 429–439.

Hill, M. W. (1974) *Biochim. Biophys. Acta 356*, 117–124.

Hubbell, W. L., Metcalfe, J. C., Metcalfe, S. M., & McConnell, H. M. (1970) *Biochim. Biophys. Acta 219*, 415–427.

Janoff, A. S., & Miller, K. W. (1982) *Biol. Membr. 4*, 417–476.

Knauf, P. (1979) *Curr. Top. Membr. Transp. 12*, 249–363.

Kotaki, A., Naoi, M., & Yagi, K. (1971) *Biochim. Biophys. Acta 229*, 547–556.

Krishnan, K. S., & Brandts, J. F. (1979) *Mol. Pharmacol. 16*, 181–188.

Lacko, L., Wittke, B., & Geck, P. (1973) *J. Cell Physiol. 83*, 267–274.

Lepke, S., Fasold, M., Pring, M., & Passow, H. (1976) *J. Membr. Biol. 29*, 147–177.

Lukacovic, M. F., Toon, M. R., & Solomon, A. K. (1984) *Biochim. Biophys. Acta 772*, 313–320.

Macara, I. G., & Cantley, L. C. (1981) *Biochemistry 20*, 5095–5105.

Makriyannis, A., & Fesik, S. W. (1980) *J. Neurosci. Res. 5*, 25–33.

Metcalfe, J. C., Seeman, P., & Burgen, A. S. V. (1968) *Mol. Pharmacol. 4*, 87–95.

Meyer, K. H. (1937) *Trans. Faraday Soc. 33*, 1062.

Miller, K. W. (1984) *Int. Rev. Neurobiol.* (in press).

Miller, K. W., Paton, W. D. M., Smith, R. A., & Smith, F. B. (1973) *Mol. Pharmcol. 9*, 131–143.

Motais, R., Baroin, A., Motais, A., & Baldy, S. (1980) *Biochim. Biophys. Acta 599*, 673–688.

Pringle, M. J., Brown, K. B., & Miller, K. W. (1981) *Mol. Pharmacol. 19*, 49–55.

Rao, A., Martin, P., Reithmeier, A. F., & Cantley, L. C. (1979) *Biochemistry 18*, 4505–4516.

Richards, C. D. (1976) *Nature (London) 262*, 534.

Richards, C. D., Martin, K., Gregory, S., Keightley, C. A., Hesketh, T. R., Smith, G. A., Warren, G. B., & Metcalfe, J. C. (1978) *Nature (London) 276*, 775–779.

Schnell, K. F. (1972) *Biochim. Biophys. Acta 282*, 265–276.

Seeman, P. (1972) *Pharm. Rev. 24*, 583–655.

Seeman, P., & Roth, S. (1972) *Biochim. Biophys. Acta 255*, 171.

Ship, S., Shami, Y., Breuer, W., & Rothstein, A. (1977) *J. Membr. Biol. 33*, 311–323.

Smith, R. A., Porter, E. G., & Miller, K. W. (1981) *Biochim. Biophys. Acta 645*, 327–338.

Trudell, J. R. (1977) *Anethesiology 46*, 5–10.

Verkman, A. S., Dix, J. A., & Pandiscio, A. A. (1981) *Anal. Biochem. 177*, 164–169.

Verkman, A. S., Dix, J. A., & Solomon, A. K. (1982) *Biophys. J. 37*, 216a.

Verkman, A. S., Dix, J. A., & Solomon, A. K. (1983) *J. Gen. Physiol. 81*, 421–449.

Waud, D. R. (1976) *Adv. Gen. Cell. Pharmacol. 1*, 145–178.

Young, A. P., & Sigman, D. S. (1981) *Mol. Pharmacol. 20*, 498–505.

Young, A. P., & Sigman, D. S. (1983) *Biochemistry 22*, 2155–2162.